


## Original Research Article

# Inhibition of MALAT1 facilitates ROS accumulation via the Keap1/HO-1 pathway to enhance photodynamic therapy in secondary hyperparathyroidism

Ying Wen<sup>a,1</sup>, Yitong Li<sup>a,b,1</sup>, Danhua Zhang<sup>a</sup>, Ziru Liu<sup>a</sup>, Hong Liu<sup>c</sup>, Xiejia Li<sup>c</sup>, Wei Wu<sup>d</sup>,  
Liyun Zeng<sup>a,\*,2</sup>, Qiongyan Zou<sup>a,\*\*,2</sup>, Wenjun Yi<sup>a,\*\*\*,2</sup> 

<sup>a</sup> Department of General Surgery, The Second Xiangya Hospital, Central South University, Clinical Research Center for Breast Disease in Hunan Province, Changsha, Hunan, 410011, China

<sup>b</sup> Breast Center, Department of General Surgery, Nanfang Hospital, Southern Medical University, Guangzhou, 510515, China

<sup>c</sup> Department of Nephrology, The Second Xiangya Hospital, Central South University, Changsha, Hunan, 410011, China

<sup>d</sup> Department of General Surgery, The Third Xiangya Hospital, Central South University, Changsha, Hunan, 410013, China



## ARTICLE INFO

## Keywords:

Secondary hyperparathyroidism  
Photodynamic therapy  
Long chain non-coding RNA  
Reactive oxygen species

## ABSTRACT

The prevalence of secondary hyperparathyroidism (SHPT) in advanced chronic kidney disease (CKD) exceeds 80 %. Our previous study indicated that photodynamic therapy (PDT) has potential for treating SHPT. Long non-coding RNA (lncRNA) is involved in various oxidative stress and apoptotic processes, but the molecular mechanism remains unreported. In this study, we found that PDT induced apoptosis in SHPT through reactive oxygen species (ROS) accumulation. The expression of metastasis-associated lung adenocarcinoma transcript 1 (MALAT1) and heme oxygenase 1 (HO-1) within SHPT was upregulated after PDT. Inhibition of MALAT1 increased PDT-induced ROS, which promoted the apoptosis. Pearson correlation analysis confirmed that there was a positive correlation between MALAT1 and HO-1, and MALAT1 inhibition down-regulated HO-1, whereas concomitant overexpression of HO-1 was able to eliminate the PDT-induced ROS and inhibit apoptosis. The direct binding of MALAT1 to Kelch-like ECH-associated protein 1 (Keap1) protein was confirmed by high-throughput sequencing, RNA pulldown, silver staining and western blotting assays. Si-Keap1 was able to rescue the down-regulation of HO-1 caused by MALAT1 inhibition, restoring the elimination of ROS by HO-1 and attenuating the effect of PDT. In addition, PDT effectively reduced parathyroid hormone (PTH) secretion in SHPT rats, and this effect was further enhanced in combination with MALAT1 inhibitors. Overall, MALAT1 activates downstream HO-1 expression by binding to Keap1, thereby reducing ROS and inhibiting apoptosis, which in turn mediates PDT resistance in SHPT. Inhibition of MALAT1 significantly enhanced the efficacy of PDT, suggesting a potential therapeutic target for improving PDT for SHPT outcomes.

## 1. Introduction

Approximately 80 % of patients with chronic kidney disease (CKD) develop secondary hyperparathyroidism (SHPT) in the late stages of the disease [1,2]. The parathyroid glands of patients with CKD are stimulated by prolonged exposure to low calcium, low magnesium, or high phosphorus levels, resulting in excessive secretion of parathyroid

hormone (PTH) [3]. The clinical manifestations of SHPT are extensive and complex, involving multiple systems including skeletal, muscular, digestive, neuropsychiatric, and cardiovascular [4]. Timely medical intervention of SHPT can effectively control disease progression, improve patients' quality of life, and reduce the risk of associated complications [5]. Conventional treatments for SHPT include pharmacological therapy, dialysis, surgery, and nutritional support [6,7]. When

\* Corresponding author.

\*\* Corresponding author.

\*\*\* Corresponding author.

E-mail addresses: [zengliyun1994@csu.edu.cn](mailto:zengliyun1994@csu.edu.cn) (L. Zeng), [zqy4311@csu.edu.cn](mailto:zqy4311@csu.edu.cn) (Q. Zou), [yiwunjun@csu.edu.cn](mailto:yiwunjun@csu.edu.cn) (W. Yi).

<sup>1</sup> These authors contributed equally to this work.

<sup>2</sup> These authors contributed equally to this work and should be considered co-corresponding authors

pharmacological treatment is ineffective or intolerable, parathyroidectomy (PTX) may become an option [8]. However, surgical treatment has limitations such as surgical complications, anesthesia risks, postoperative hypocalcemia, and recurrence [9]. Therefore, exploring less invasive, broader-spectrum, and fewer side-effect treatment methods is particularly important and urgent.

Photodynamic therapy (PDT) is a low-invasive treatment method that uses specific photosensitizers, which, when irradiated with particular wavelengths of light, generate large amounts of reactive oxygen species (ROS) within the tissue, leading to local tissue damage [10]. The 5-aminolevulinic acid (5-ALA) is the most widely used and classic photosensitizer [11]. As a precursor substance in heme biosynthesis, its metabolic intermediate protoporphyrin IX (PpIX) exhibits photosensitive effects [12]. Due to the slow rate of metabolism of ferrochelatase (FECH) in the parathyroid glands, PpIX tends to accumulate there compared to surrounding tissues [13], allowing PDT to precisely target the parathyroid glands. The cytotoxicity induced by PDT is primarily driven by ROS, which are highly reactive oxidizing substances, including superoxide anions, hydrogen peroxide, and hydroxyl radicals [14]. These highly reactive oxidizing substances react with biomolecules such as lipids, proteins, and DNA within cells, causing oxidative damage, thereby inducing cell death [15]. PDT directly inhibits local tumors through minimally invasive strategies, but it seems unable to achieve complete eradication and prevent metastasis and recurrence [16]. Cells can protect themselves against cytotoxic products by increasing antioxidant mechanisms and repair capacity, and one of the reasons for PDT resistance is the reduction of intracellular ROS [17].

The interaction between long non-coding RNA (lncRNA) and ROS has been confirmed in various cellular environments [18]. Identifying lncRNA that interact with ROS provides new potential targets for the treatment of oxidative stress and ROS dysregulation-related diseases [19]. Additionally, lncRNA regulates the efficacy of PDT by affecting the stability, cellular uptake, and local release of photosensitizers, as well as ROS during the photosensitive effect [20].

In our study, despite the large concentration of photosensitizers, ROS levels still have a plateau, which may be the reason for the insufficient PDT efficacy. We found that the levels of metastasis associated lung adenocarcinoma transcript 1 (MALAT1) were significantly upregulated after PDT in SHPT. Therefore, we propose a hypothesis that MALAT1 may be involved in the regulation of oxidative stress in SHPT during PDT, thereby affecting its efficacy. This study is expected to elucidate the molecular mechanism of PDT resistance and provide a strong experimental basis for optimizing the efficacy of PDT and its future clinical application.

## 2. Methods

### 1 Isolation and culture of SHPT primary cells

In China, the indication for PTX in SHPT patients is a persistent serum PTH level higher than 875 pg/mL with one or more severe complications [21]. Sixty SHPT patients were recruited in this study. Surgically excised parathyroid glands were washed, cut, digested, separated, filtered, centrifuged, and the cell precipitate was collected under aseptic operation [22,23]. SHPT primary cells were incubated in RPMI 1640 medium supplemented with 10 % fetal bovine serum (FBS) and 1 % penicillin/streptomycin and cultured at 37 °C with 5 % CO<sub>2</sub>. Subsequently, the cells were photodynamically treated according to the steps described in our previous paper [23].

### 2 Cell transfection

Antisense oligonucleotides (ASO) for MALAT1 and siRNA for heme oxygenase 1 (HO-1) were provided by RiboBio (Guangzhou, China), which were transfected into SHPT primary cells with Lipofectamine™ 2000 (Thermo Fisher, USA) according to the producer's instructions.

The cells were collected 48 h later to verify the interference in the gene.

### 3 Screening of differentially expressed genes (DEGs)

After total RNA was extracted from the samples and rigorously examined for quality and purity, and a cDNA library was established, a large amount of bipartite sequencing data was obtained through the Illumina sequencing platform, and the FPKM method was used to analyze the RNA expression levels. Then, the DEGs were calculated using the DESeq R package. The DEGs of the dataset with an absolute log<sub>2</sub> fold change (FC) > 1 and an adjusted P value of < 0.05 were considered for subsequent analysis.

### 4 Detection of half maximal inhibitory concentration (IC<sub>50</sub>) for 5-ALA

SHPT cells were plated in 96-well plates in 100 µl RPMI-1640 medium, and cultured for varying 5-ALA (Aladdin, China) concentration for 12h. A total of 10 µl CCK8 reagent (Biosharp, China) was added into the cells, followed by the incubation of 2 h at 37 °C. The absorbance at 450 nm was measured using a microplate reader (Thermo Scientific Multiskan FC, USA).

### 5. Quantitative reverse transcription-polymerase chain reaction (qRT-PCR)

TRIzol reagent (Invitrogen, USA) was used to isolate RNA from cells and tissues. Ribo™ mRNA/lncRNA qRT-PCR Starter Kit (RiboBio, China) was used to perform reverse transcription and qRT-PCR. The 2<sup>-ΔΔCt</sup> method was used for the calculation of relative levels of genes normalized to GAPDH. The sequences of primers used are presented in Table 1.

### 6 Western blotting

SHPT primary cells were lysed using RIPA buffer (Beyotime, China) supplemented with phenylmethylsulfonyl fluoride (PMSF), incubated on ice for 30 min, and centrifuged at 4 °C for 15 min at 12,000 rpm. Protein samples were separated by electrophoresis in a 12 % SDS-PAGE gel and then transferred to polyvinylidene difluoride (PVDF) membranes, which were then blocked with 5 % non-fat milk for 60 min. The membranes were incubated with primary antibody at 4 °C overnight and incubated with secondary antibodies respectively at room temperature for 60 min. The enhanced chemiluminescence (ECL) system was used to visualize the protein bands, and the intensity of bands were measured by Image J.

The primary antibodies used were as follows: HO-1 (10701-1-AP, Proteintech), Keap1 (10503-2-AP, Proteintech), Caspase-3 (19677-1-AP, Proteintech), Caspase-8 (13423-1-AP, Proteintech), Caspase-9 (10380-1-AP, Proteintech), BAX (60267-1-Ig, Proteintech), BAD (10435-1-AP, Proteintech), BCL2 (68103-1-Ig, Proteintech) and β-actin (66009-1-Ig, Proteintech).

**Table 1**

Primer sequences used for qRT-PCR analysis in this study.

Genes		Sequence
MALAT1	Forward	GGTGTACACAGAAGTGGATTTCAG
	Reverse	TGCTCGCTTGCTCCTCAGTC
HO-1	Forward	TGCCAGTGCCACCAAGTTCAAG
	Reverse	TGTTGAGCAGGAACGCAGTCTTG
Keap1	Forward	GCTGTCCTCAATCGTCTCCTTTATG
	Reverse	TCATTGCGCACTCGTTCCTCTC
Nrf2	Forward	TTCCCTCAGCAGCATCCTCTCC
	Reverse	AATCTGTGTTGACTGTGGCATCTG
GAPDH	Forward	TGACTTCAACAGCGACACCCA
	Reverse	CACCCTGTTGCTGTAGCCAAA

## 7 Detection of Reactive Oxygen Species (ROS)

The level of ROS was analyzed in each group of SHPT primary cells after PDT using the Reactive Oxygen Species Kit (Beyotime, China). The treated SHPT primary cell suspensions (10,000 cells/100  $\mu$ L/well) were inoculated into 96-well plates, and incubated with 5-ALA without light for more than 8 h. After PBS washing, the cells were incubated in medium containing DCFH-DA at 37 °C for 30 min, and immediately irradiated using a photodynamic apparatus, and then observed by a fluorescence microscope (Zeiss LSM700, Germany).

## 8 TdT-mediated dUTP Nick-End Labeling (TUNEL) staining

SHPT primary cells were inoculated into 96-well plates and photodynamically irradiated under different experimental conditions. The TUNEL assay solution was prepared according to the instructions of the One Step TUNEL Apoptosis Assay Kit (Beyotime, China) to incubate the cells at 37 °C for 60 min without light, which were observed by a fluorescence microscopy (Zeiss LSM700, Germany).

## 9 Flow cytometry

Photodynamically treated cells were harvested and treated with 0.25 % trypsin without ethylenediaminetetraacetic acid for digestion, followed by centrifugation for 5 min and resuspended in the binding buffer (200  $\mu$ L). Then, 5  $\mu$ L Annexin V-fluorescein isothiocyanate (FITC) and 10  $\mu$ L propidium iodide (PI, Cell Signaling Technology, USA) were added and stored at room temperature without light for 30 min. Apoptosis was analyzed using a flow cytometry (BD Biosciences, USA).

## 10 RNA Pulldown assay and Silver staining

RNA Pulldown was performed using the Pierce™ Magnetic RNA-Protein Pulldown Kit (Thermo Fisher, USA). Biotin-labeled sense and antisense MALAT1 probes were supplied by Genecreate Biological Engineering Co., LTD. The probes were mixed with streptavidin beads (Thermo Fisher, USA) in total cell lysate and shaken at 4 °C overnight. After elution of the RNA-protein complexes with Elution Buffer, the pulled-down proteins were upsampled into a 12 % SDS-PAGE gel and analyzed by silver staining and western blotting. Silver staining assay was conducted by Fast Silver Stain Kit (Biosharp, China) according to the manufacturer's protocol.

## 11 Establishment of SHPT rats

Animal experiments were approved by the Laboratory Animal Welfare Ethics Committee of the Second Xiangya Hospital. The Sprague–Dawley rats (n = 24) aged 8 weeks were purchased from Hunan Slac Jingda Laboratory Animal Co., Ltd. The SHPT rats were established by 5/6 nephrectomy combined with high phosphorus feeding [24]. The level of serum intact PTH was detected before and after operation using a Bioactive Intact PTH ELISA kit (AiFang Biological, China). MALAT1 inhibitor (MALAT1i) was purchased from MedChemexpress (HY-115579, USA).

## 12 Hematoxylin and Eosin (HE) staining and Immunohistochemistry (IHC)

According to previous study [25], SHPT rats were anesthetized and injected intraperitoneally with 5-ALA (300 mg/kg), 2h later the parathyroid region was exposed and irradiated using a 405 nm laser, and the parathyroid glands to appear red fluorescence. Subsequently, after each group of rats was treated according to different conditions, their parathyroid, heart, liver, spleen, lung and kidney tissues were collected and fixed in formalin overnight. After paraffin embedding, the sections were stained using Hematoxylin and Eosin Staining Kit (Beyotime, China).

IHC was performed using the UltraSensitive™ S-P kit (Maixin, China) as per the manufacturer's protocol. The results were observed and imaged under a microscope.

## 13 Statistical analysis

Graphs and statistical analyses were performed with Graph Pad Prism 9. Student t-test was used between two groups, and one-way ANOVA followed by Tukey's post hoc test was utilized for comparing more than two groups. Data are presented as mean  $\pm$  standard deviation,  $P < 0.05$  was considered statistically significant.

## 3. Results

### 1 5-ALA-PDT-dependent accumulation of ROS induces apoptosis in SHPT

To investigate the effect of 5-ALA-PDT on SHPT, we performed western blotting on SHPT primary cells treated with different concentrations of 5-ALA-PDT. The results showed that the expression of proapoptotic proteins BAX, BAD and Caspase family proteins were significantly upregulated (Fig. 1A, sFig. 1A). Moreover, we set multiple 5-ALA concentrations (0.03125, 0.0625, 0.125, 0.25, 0.5, 1, and 2 mM/L) to incubate SHPT primary cells, and the IC50 of SHPT primary cells for 5-ALA-PDT was 0.054 mM/L (Fig. 1B). Thus, for subsequent studies we chose 0.0625 mM/L as the incubation concentration for 5-ALA. Notably, despite the incubation concentration of 5-ALA exceeded the IC50, the increase in pro-apoptotic protein levels was no longer dependent on the dose of 5-ALA, and SHPT cells could still maintain a certain level of viability (Fig. 1A and B), which implies that part of the cells was insensitive to PDT.

We further examined the levels of intracellular ROS with different concentrations of 5-ALA-PDT. The levels of ROS increased with increasing 5-ALA incubation concentration (Fig. 1C). However, when the 5-ALA incubation concentration exceeded 0.25 mM/L, the intracellular ROS level entered a plateau period. Subsequently, we used N-Acetyl-L-cysteine (NAC) to eliminate ROS, PDT-induced increased BAX, BAD, and Caspase family proteins were reduced to different degrees after NAC treatment (Fig. 1D–sFig. 1B). In addition, a significant increase in ROS was observed after 5-ALA-PDT, and the use of NAC inhibited PDT-induced ROS (Fig. 1E).

### 2 MALAT1 inhibition enhances 5-ALA-PDT-induced ROS and apoptosis

We analyzed the expression profiles of lncRNAs in SHPT cells before and after PDT. We highlighted up-regulated genes in red and down-regulated genes in blue/green in the heatmap (Fig. 2A) and volcano plot (Fig. 2B). Among them, 523 lncRNAs were upregulated and 323 lncRNAs were downregulated. Subsequently, qRT-PCR assay suggested that the difference was most pronounced for MALAT1 after 5-ALA-PDT (Fig. 2C). Consistent results were also observed in parathyroid tissue of photodynamically treated SHPT rats (Fig. 2D). We transiently transfected two ASOs targeting MALAT1 into SHPT primary cells, and qRT-PCR verified that the interference efficiency of the ASOs was above 60 % (Fig. 2E). PDT in combination with MALAT1 ASO-1 or ASO-2 resulted in a further increase in the levels of the pro-apoptotic factors BAX, BAD, and Cleaved caspase3, while the opposite was observed for the anti-apoptotic molecule BCL2 (Fig. 2F–sFig. 1C). The inhibition of MALAT1 further increased ROS levels and apoptosis induced by 5-ALA-PDT (Fig. 2G and H, sFigure 1D&E).

We used the method of “5/6 nephrectomy + high phosphorus feeding” to construct the SHPT rat model (Fig. 3A). Serum calcium, phosphate, creatinine (CR), blood urea nitrogen (BUN), and iPTH were significantly elevated as well as obviously emaciated in SHPT rats (sFig. 1F). 5-ALA-PDT significantly reduced serum iPTH in SHPT rats,

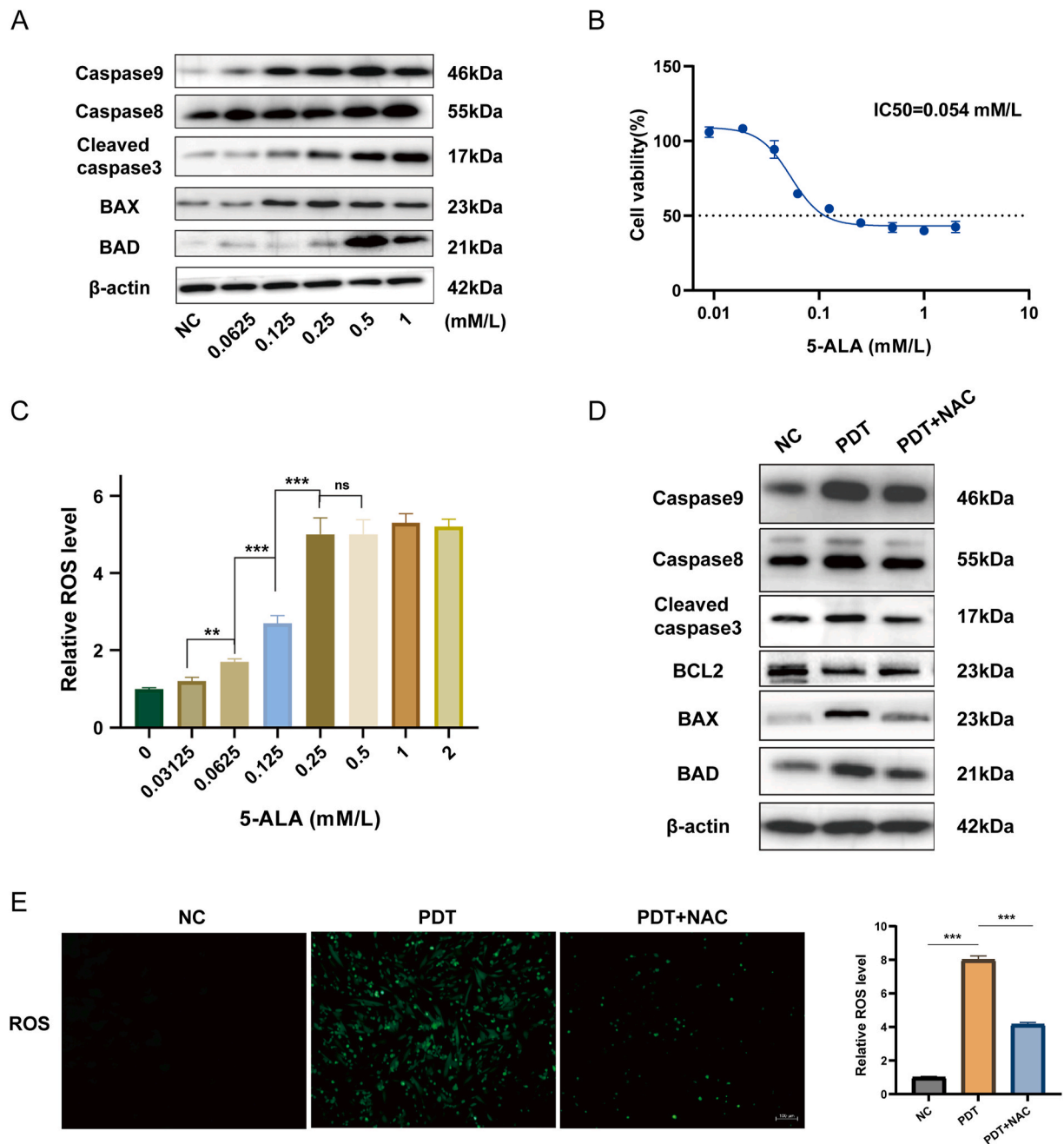


**Fig. 1.** 5-ALA-PDT-dependent accumulation of ROS induces apoptosis in SHPT. (A) The expressions of apoptosis-related proteins were assessed by western blotting. (B) Determination of IC50 of SHPT primary cells for the photosensitizer 5-ALA by CCK8 assay. (C) The relative level of ROS in SHPT primary cells during 5-ALA-PDT. (D) The expressions of apoptosis-related proteins were assessed by western blotting. (E) The levels of ROS in SHPT primary cells at different conditions; scale bar: 100  $\mu$ m. NAC, N-Acetyl-L-cysteine; NC, non-specific control. \* $P < 0.05$ ; \*\* $P < 0.01$ ; \*\*\* $P < 0.001$ ; ns, no significance.

and concomitant inhibition of MALAT1 further reduced its level (Fig. 3B). Similarly, disruption of glandular structure and reduction of PTH secretion were observed in the parathyroid glands of SHPT rats after 5-ALA-PDT, which was enhanced by concomitant combination of MALAT1 inhibitors (Fig. 3C). We simultaneously observed the safety of MALAT1 inhibitor on important organs (including heart, liver, spleen, lung and kidney) in rats (Fig. 3D).

### 3 MALAT1 affects the efficacy of 5-ALA-PDT by regulating HO-1

Our further differential analysis and RT-qPCR both indicated that HO-1 was significantly up-regulated after 5-ALA-PDT (Fig. 4A and B). Pearson correlation analysis showed a positive correlation between the

expression of MALAT1 and HO-1 after 5-ALA-PDT ( $r = 0.9758, p < 0.01$ ) (Fig. 4C). The MALAT1 knockdown caused suppressed levels of HO-1 RNA transcription (Fig. 4D) and protein expression (Fig. 4E–sFig. 2A). Hemin is an effective HO-1 inducer, and western blotting confirmed that the protein level of HO-1 increased accordingly with the increase of Hemin concentration (Fig. 4F–sFig. 2B), as well as the siRNAs of HO-1 were effective in interfering with its expression level (Fig. 4G–sFig. 2C). Subsequently, we examined the effect of HO-1 on ROS and apoptosis during 5-ALA-PDT using an inducer (Hemin) and an inhibitor (Zinc Protoporphyrin, ZnPP) of HO-1, respectively [26–28]. 5-ALA-PDT induced a large amount of intracellular ROS, which was significantly reduced by overexpression of HO-1, and the opposite result for inhibition of HO-1 (Fig. 4H). Consistent results were also observed

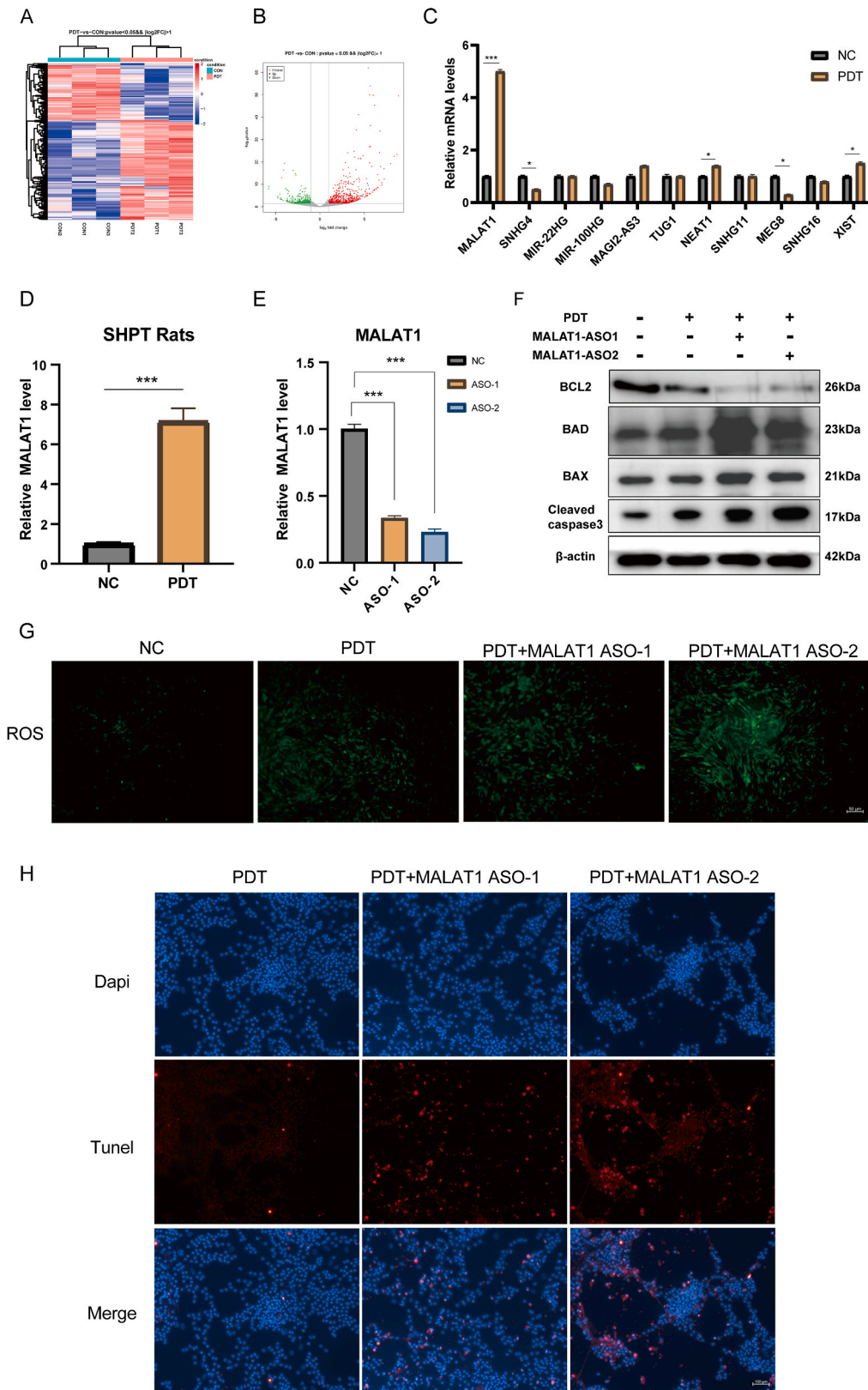


**Fig. 2. MALAT1 inhibition enhances 5-ALA-PDT efficacy.** (A) Heatmap and (B) volcano plot analysis of differentially expressed lncRNAs during 5-ALA-PDT in SHPT. (C) The levels of lncRNAs during 5-ALA-PDT in parathyroid tissue of SHPT patients by qRT-PCR. (D) The levels of MALAT1 before and after 5-ALA-PDT in SHPT rats. (E) The expression of MALAT1 in knockdown groups by qRT-PCR. (F) The expressions of apoptosis-related proteins were assessed by western blotting. (G) The levels of ROS in SHPT primary cells at different conditions; scale bar: 50  $\mu$ m. (H) The levels of apoptosis in SHPT primary cells at different conditions by TUNEL assay; scale bar: 100  $\mu$ m. NC, non-specific control. \* $P < 0.05$ ; \*\* $P < 0.01$ ; \*\*\* $P < 0.001$ ; ns, no significance.

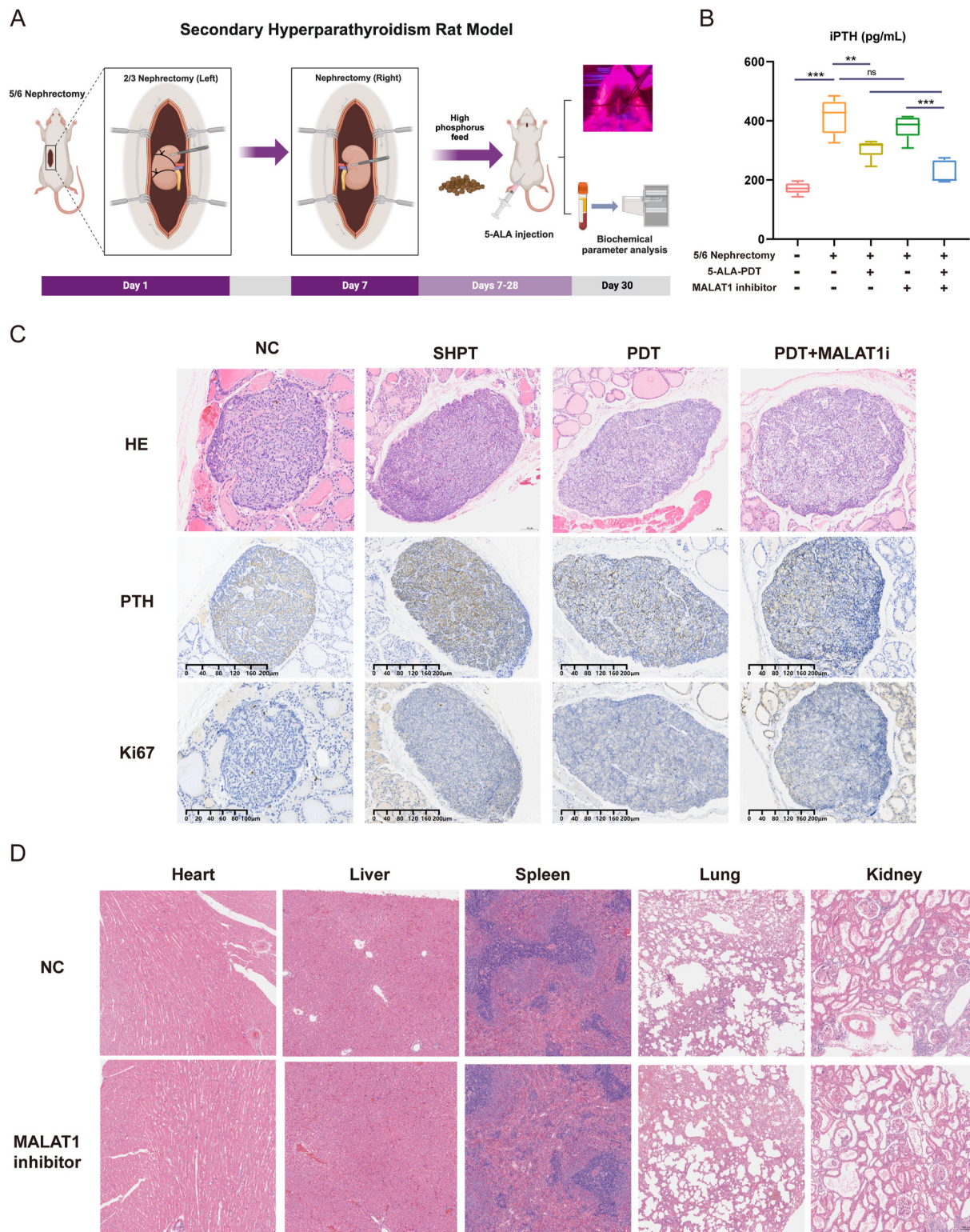


**Fig. 3. Construction and characterization of an experimental secondary hyperparathyroidism (SHPT) model in rats.** (A) The experimental design for the 5/6 nephrectomy and high phosphorus feeding rat model. (B) The levels of iPTH in SHPT rats at baseline, pre-PDT, post-PDT, and MALAT1 inhibitor. (C) The microstructure of the parathyroid glands of SHPT rats showed by HE staining, and the expression of PTH and Ki67 detected by immunohistochemical; scale bar: 200  $\mu$ m. (D) Morphology studies in heart, liver, spleen, lung and kidney of the SHPT model versus NC in rat. NC, non-specific control. \* $P < 0.05$ ; \*\* $P < 0.01$ ; \*\*\* $P < 0.001$ ; ns, no significance.

using HO-1 siRNAs, i.e., ROS levels increased significantly after knockdown of HO-1 (Fig. 4I). Flow cytometry, TUNEL assay and western blotting revealed that overexpression of HO-1 suppressed 5-ALA-PDT-induced apoptosis. Conversely, inhibition of HO-1 enhanced

5-ALA-PDT-induced apoptosis (Fig. 5A–C, sFigure 3A&B). Subsequently, by performing rescue experiments with simultaneous inhibition of MALAT1 and overexpression of HO-1, we found that overexpression of HO-1 rescued the increase of ROS and apoptosis caused by inhibition of

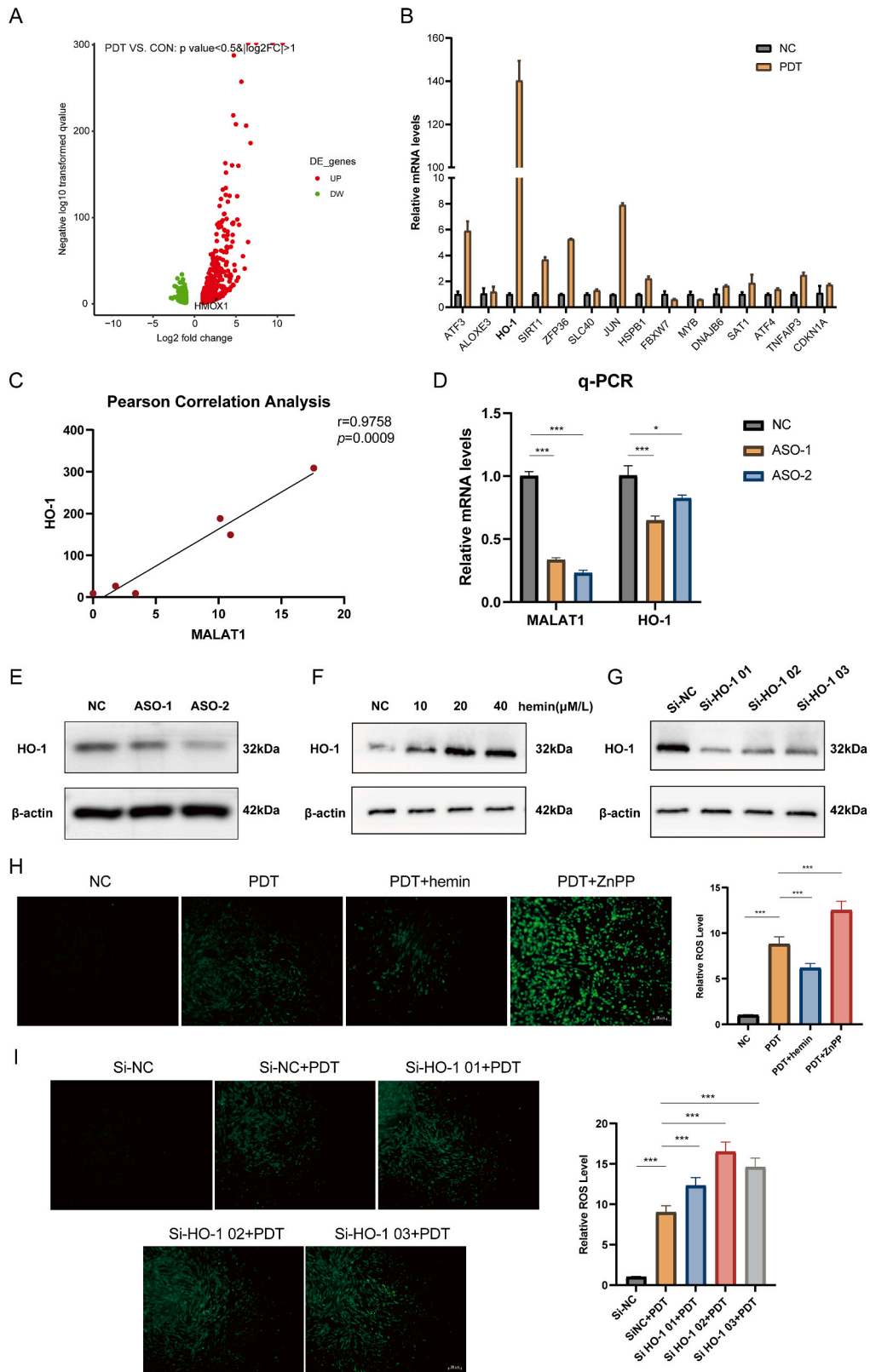


**Fig. 4. MALAT1 regulates HO-1 to affect the ROS induced by 5-ALA-PDT in SHPT.** (A) Volcano plot analysis of differentially expressed mRNAs during 5-ALA-PDT in SHPT. (B) The levels of mRNAs during 5-ALA-PDT in parathyroid tissue of SHPT patients by qRT-PCR. (C) The association between MALAT1 and HO-1. (D) qRT-PCR verified changes in HO-1 mRNA levels after knockdown of MALAT1. (E, F, G) The expressions of HO-1 were assessed at different conditions by western blotting. (H, I) The levels of ROS in SHPT primary cells at different conditions; scale bar: 50  $\mu$ m. NC, non-specific control. \* $P < 0.05$ ; \*\* $P < 0.01$ ; \*\*\* $P < 0.001$ ; ns, no significance.

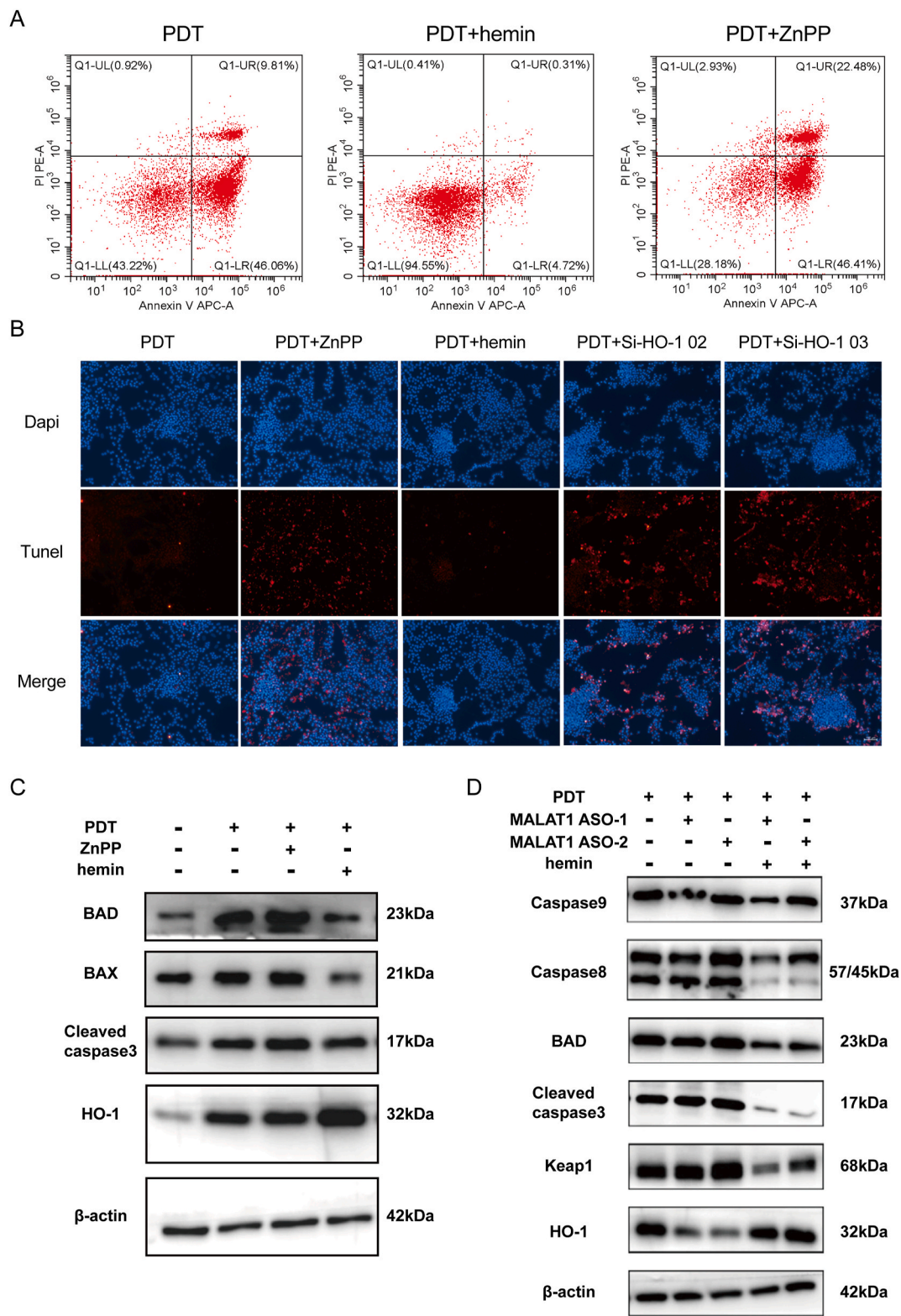


**Fig. 5. MALAT1 regulates HO-1 to affect apoptosis induced by 5-ALA-PDT.** (A) The proportions of apoptosis induced by PDT upon overexpression and inhibition of HO-1 by flow cytometry. (B) The levels of apoptosis in SHPT primary cells at different conditions by TUNEL assay; scale bar: 100 μm. (C, D) The expressions of apoptosis-related proteins were assessed by western blotting.

MALAT1 (Figs. 5D and 6A&B, sFigure 3C&D).

#### 4 MALAT1 targets Keap1 to regulate HO-1

One of the key pathways involved in HO-1 is the Kelch-like ECH-

associated protein 1 (Keap1)/nuclear-factor-E2-related factor 2 (Nrf2) signaling pathway, which is a crucial intracellular antioxidant response mechanism responsible for regulating cellular response and modulation to oxidative stress [29]. We found that inhibition of MALAT1 resulted in no significant difference in the RNA transcript levels of Keap1, while



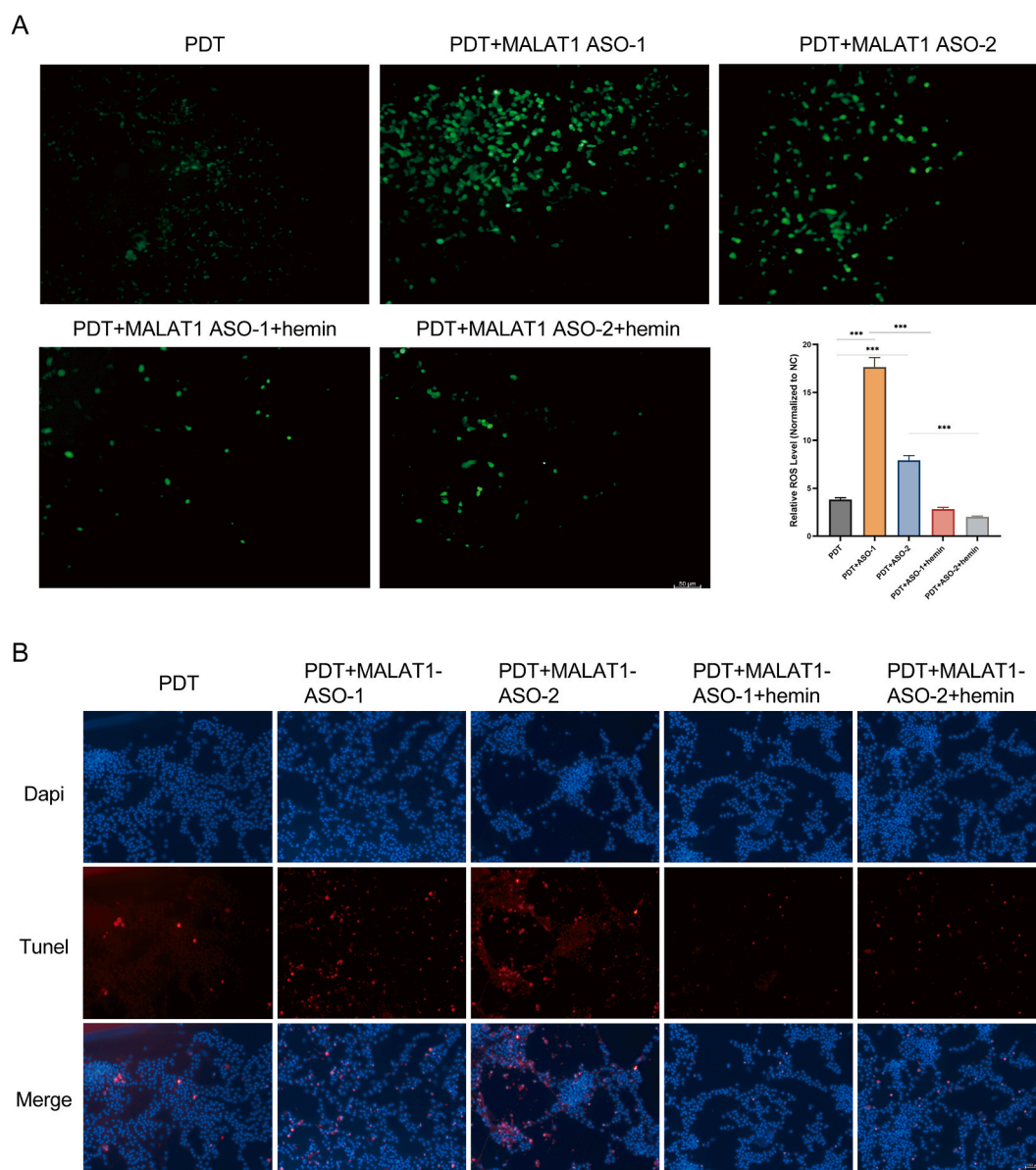


**Fig. 6.** Overexpression of HO-1 reversed the increase in ROS and apoptosis induced by MALAT1 inhibition in 5-ALA-PDT. The levels of ROS (A, scale bar: 50  $\mu$ m) and apoptosis (B, scale bar: 100  $\mu$ m) upon simultaneous suppression of MALAT1 and overexpression of HO-1 during 5-ALA-PDT in SHPT primary cells. \*\*\* $P < 0.001$ .

protein expression levels were significantly up-regulated, while both RNA and protein levels of Nrf2 were down-regulated (Fig. 7A and B, sFig. 4A). RNA pull-down and protein fast silver staining assay revealed that the Keap1 was pulled down by the MALAT1 sense probe, suggesting that it was interacted with lncRNA MALAT1 (Fig. 7C). Consistently, RNA pull-down assays followed by western blotting exhibited the enrichment of Keap1 protein in the complex of MALAT1 in SHPT cells, confirming that Keap1 protein rather than Nrf2 protein bound to MALAT1 (Fig. 7D).

Moreover, we utilized chloroquine (CQ) and MG132 to inhibit degradation of Keap1 protein by two pathways: the autophagy-lysosome and ubiquitin-proteasome dependent degradation pathways, respectively [30–32]. Keap1 protein levels were upregulated following inhibition of MALAT1, and the addition of MG132 further increased this effect; however, CQ did not seem to have an effect on this (Fig. 7E–sFig. 4B). Subsequently, we used cycloheximide (CHX) to inhibit cellular protein synthesis, and MALAT1-ASO reversed the inhibition of Keap1 by CHX in a time-dependent manner, and also further amplified the inhibition of the ubiquitination of Keap1 by MG132

(Fig. 7F), these results confirm that MALAT1 regulates Keap1 through the ubiquitin-proteasome pathway.

#### 5 Silencing Keap1 reversed the increase in ROS and apoptosis induced by MALAT1 inhibition in 5-ALA-PDT

Si-Keap1 significantly silenced the elevation of Keap1 protein caused by MALAT1-ASO, while it could restore the expression level of HO-1, and this difference was statistically significant (Fig. 8A, sFig. 4C). Inhibition of MALAT1 increased 5-ALA-PDT-induced ROS, while silencing of Keap1 reversed the increase in ROS (Fig. 8B). The results of apoptosis were also consistent with it, inhibition of MALAT1 increased 5-ALA-PDT-induced apoptosis, while silencing Keap1 reversed the level of apoptosis (Fig. 8C–sFig. 4D). Overall, MALAT1 targeting of Keap1 resulted in the release of Nrf2, upregulated HO-1 to eliminate ROS, and ultimately attenuated the efficacy of PDT (Fig. 8D).

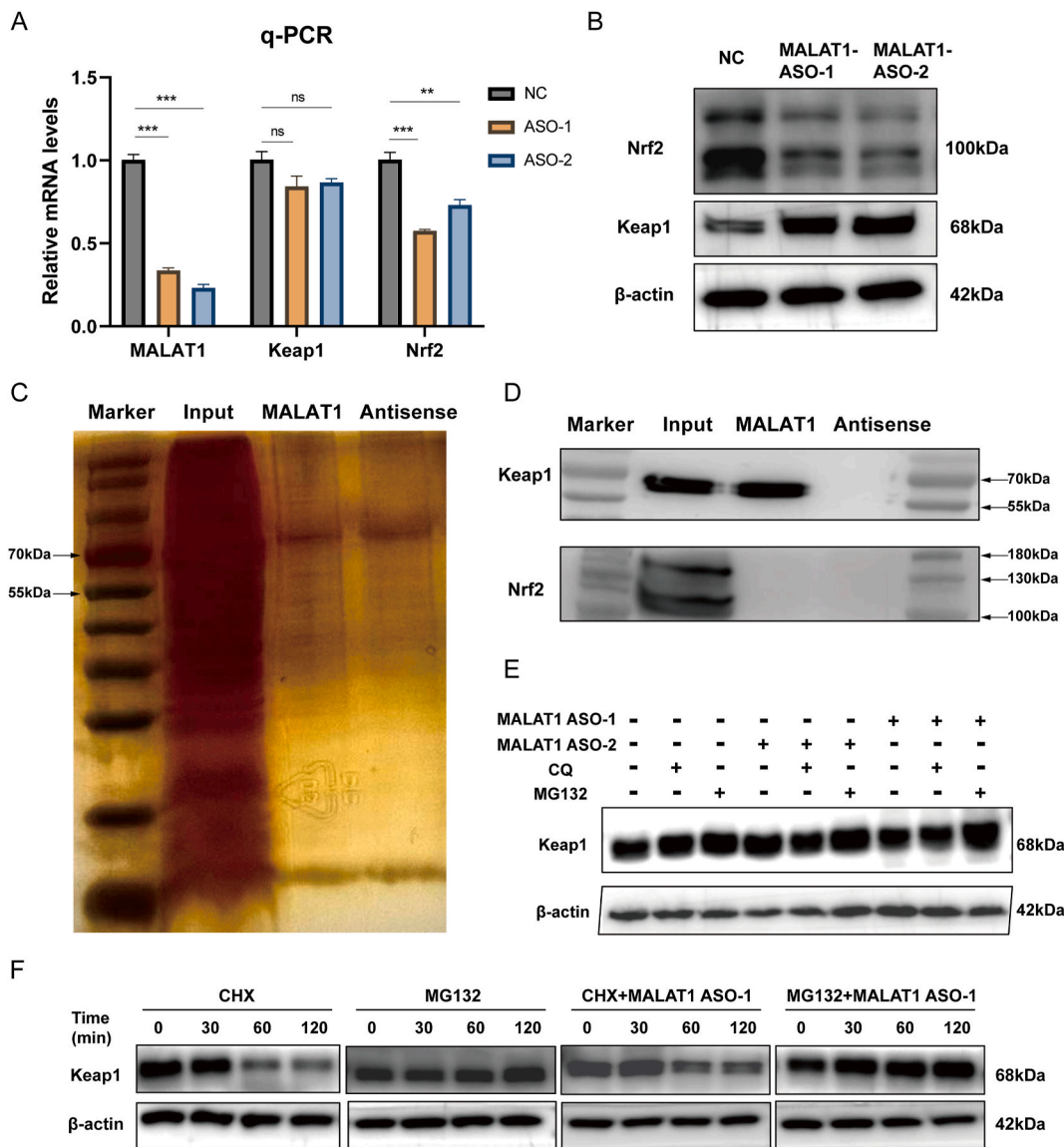


**Fig. 7. MALAT1 targets Keap1 to regulate HO-1.** The RNA (A) and protein (B) expression of Keap1 and Nrf2 after inhibiting MALAT1. (C) Pull-down assays followed by silver staining assay determined the interacted proteins of MALAT1. (D) RNA pull-down followed by western blotting showed the Keap1 level in the complex of sense or antisense MALAT1. (E, F) The expressions of Keap1 were assessed at different drug (CQ, MG132, CHX and/or MALAT1-ASO) stimuli by western blotting. CQ, chloroquine; CHX, cycloheximide; NC, non-specific control. \*\*P < 0.01; \*\*\*P < 0.001; ns, no significance.

**4. Discussion**

Photodynamic therapy, as a non-invasive clinical treatment method, has multiple significant advantages [33,34]. Firstly, its non-invasive nature avoids surgery or incision, significantly reducing patient discomfort and shortening recovery time [35]. Secondly, PDT can achieve precise targeting and treatment of specific lesions while having minimal impact on surrounding healthy tissues, thereby reducing the risk of side effects and complications during treatment [36,37]. Thirdly, PDT is repeatable, allowing for multiple treatments without cumulative toxicity or damage [38].

LncRNA MALAT1 is highly expressed in a variety of tumors and is closely associated with tumorigenesis, progression, metastasis, chemoresistance and prognosis [39]. MALAT1 is closely involved in the regulation of ROS, e.g., overexpression of MALAT1 significantly reduces ROS levels and improves cerebral infarction and cognitive dysfunction in cerebral ischemia-reperfusion mice [40]. HO-1 is a key intracellular enzyme involved in an important step of the hemoglobin metabolism pathway [41]. It inhibits the production and activity of ROS, thereby

reducing cellular oxidative damage [42,43]. HO-1 influences ROS levels indirectly by catalyzing the breakdown of hemoglobin and releasing free iron ions [44]. Additionally, HO-1 has anti-inflammatory effects, reducing the increase of intracellular ROS caused by inflammation [45].

In this study, we clarified that the MALAT1/Keap1/HO-1/ROS axis leads to PDT resistance, which not only provides new insights for the treatment of SHPT but also for other diseases treated by PDT. Under normal circumstances, Nrf2 is bound to Keap1 and exposed to ubiquitin-dependent degradation [46]. However, when cells are subjected to oxidative stress, ionizing radiation, or chemical stimuli, Keap1 becomes inactive, leading to the release of Nrf2 [47]. Previous studies have reported the influence of MALAT1 on ROS production. Rong Zeng et al. found that LV-MALAT1 induces the downregulation of Keap1, leading to the stabilization and activation of Nrf2, which in turn reduces ROS production and protects human umbilical vein endothelial cells (HUVECs) from oxidative damage [48]. Our research indicates that apoptosis induced by PDT in SHPT is primarily driven by ROS and is accompanied by the BCL2 and caspase family apoptosis cascades. PDT increased the expression of MALAT1, which inhibited Keap1 by binding

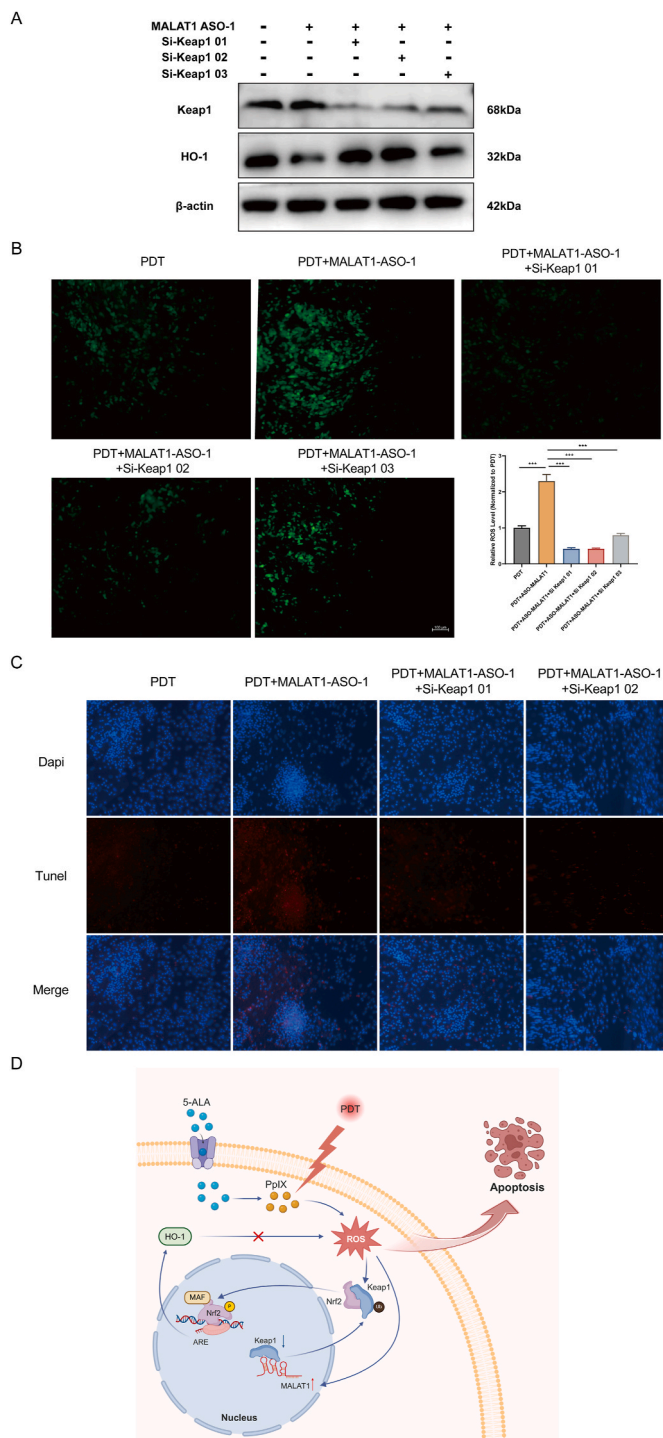


**Fig. 8. Silencing Keap1 reversed the increase in ROS and apoptosis induced by MALAT1 inhibition in 5-ALA-PDT.** (A) The expressions of apoptosis-related proteins were assessed upon simultaneous inhibition of MALAT1 and Keap1 by western blotting. The levels of ROS (B, scale bar: 50 μm) and apoptosis (C, scale bar: 100 μm) upon simultaneous inhibition of MALAT1 and Keap1 during 5-ALA-PDT in SHPT primary cells. (D) The schematic diagram of the mechanisms of MALAT1/Keap1/HO-1/ROS to regulate PDT resistance in SHPT.

to it, preventing it from effectively capturing Nrf2. This allows Nrf2 to be released into the nucleus, where it forms heterodimers with one of the small Maf proteins and recognize antioxidant response elements (ARE), initiating downstream HO-1 transcription [49]. This process inhibits ROS and apoptosis induced by PDT, thereby affecting the efficacy of

PDT.

Similar to our findings, a prior study on a murine xenograft model of human multiple myeloma demonstrated that LNA-gapmer antisense oligonucleotide antagonizes MALAT1, promoting KEAP1 transcriptional activation and reducing the expression of the proteasome subunits' key transcriptional activators Nrf1 and Nrf2, leading to reduced antioxidant gene expression and increased ROS levels [50]. However, an opposing result was reported in diabetic retinopathy models, where downregulation of MALAT1 by siRNA prevented glucose-induced increases in Keap1 and facilitated Nrf2 nuclear translocation, which is essential for activating antioxidant genes (HO-1 and Sod2), thereby protecting the retina from oxidative damage [51]. Additionally, another study found that overexpression or knockdown of MALAT1 had no significant impact on ROS production in human brain microvascular endothelial cells under oxygen-glucose deprivation and reoxygenation conditions [52].

These contrasting observations suggest that the role of MALAT1 in the Keap1/Nrf2/ROS axis may involve complex regulatory mechanisms that vary across cellular contexts and disease models. We hypothesize that this could be similar to the dual role of autophagy in cell metabolism and physiology, where it can function as both a survival mechanism and a pathway for cell death, depending on the cellular environment and signaling pathways involved [53,54]. It is possible that multiple pathways modulate ROS levels by MALAT1, potentially resulting in either an increase or reduction in ROS levels due to these “competitive” interactions. Further studies are needed to clarify these mechanisms.

There are limitations to this study. Firstly, we need to construct multiple truncated or mutated probes of the MALAT1 sequence to identify the binding regions of Keap1. Secondly, exploring the interaction domains between Keap1 protein and MALAT1 can provide a more comprehensive understanding of the binding mechanism. Additionally, the specific mechanism by which MALAT1 regulates the ubiquitination of Keap1 remains unclear and requires further exploration.

In conclusion, MALAT1 downregulates Keap1 by directly binding to it, subsequently upregulating HO-1, scavenging ROS, inhibiting apoptosis and attenuating PDT efficacy. This provides a theoretical basis for targeting MALAT1 as a clinical application of PDT to treat SHPT and optimize its efficacy.

#### CRedit authorship contribution statement

**Ying Wen:** Writing – original draft, Validation, Formal analysis, Conceptualization. **Yitong Li:** Visualization, Methodology, Data curation. **Danhua Zhang:** Resources, Methodology, Investigation. **Ziru Liu:** Software, Methodology, Investigation. **Hong Liu:** Resources, Data curation. **Xiejia Li:** Resources, Data curation. **Wei Wu:** Validation, Supervision. **Liyun Zeng:** Writing – review & editing, Validation, Methodology. **Qiongyan Zou:** Writing – review & editing, Project administration, Conceptualization. **Wenjun Yi:** Writing – review & editing, Funding acquisition, Conceptualization.

#### Ethics approval and consent to participate

The study protocol was reviewed and approved by the Medical Ethics Committee of the Second Xiangya Hospital of Central South University (2020 Lun Shen [Professional Research] No. 002) and was in accordance with the Declaration of Helsinki. All participants signed a written informed consent.

The Animal Ethical and Welfare Committee of the Second Xiangya Hospital of Central South University (Approval No.20230399) approved all the animal experiments.

#### Consent for publication

All authors agree to the submission and publication of the manuscript.

## Availability of data and material

The data that support the findings of this study are available on request from the corresponding author.

## Funding

This research was supported by the National Natural Science Foundation of China (82270834).

## Abbreviations List

5-ALA	5-aminolevulinic acid
ARE	Antioxidant response elements
ASO	Antisense oligonucleotides
BUN	Blood urea nitrogen
CHX	Cycloheximide
CKD	Chronic kidney disease
CQ	Chloroquine
CR	Creatinine
ECL	Enhanced chemiluminescence
FBS	Fetal bovine serum
FECH	Ferrochelatase
FITC	Fluorescein isothiocyanate
HE	Hematoxylin and Eosin
HO-1	Heme oxygenase 1
IC50	Half maximal inhibitory concentration
IHC	Immunohistochemistry
Keap1	Kelch-like ECH-associated protein 1
lncRNA	Long noncoding RNA
MALAT1	Metastasis-associated lung adenocarcinoma transcript 1
NAC	N-Acetyl-L-cysteine
Nrf2	Nuclear-factor-E2-related factor 2
PDT	Photodynamic therapy
PMSF	Phenylmethylsulfonyl fluoride
PTH	Parathyroid hormone
PTX	Parathyroidectomy
PVDF	Polyvinylidene difluoride
qRT-PCR	Quantitative reverse transcription-polymerase chain reaction
ROS	Reactive oxygen species
SHPT	Secondary hyperparathyroidism
TUNEL	TdT-mediated dUTP Nick-End Labeling
ZnPP	Zinc Protoporphyrin

## Appendix A. Supplementary data

Supplementary data to this article can be found online at <https://doi.org/10.1016/j.ncrna.2024.12.001>.

## References

- [1] M. Ketteler, G.A. Block, P. Evenepoel, M. Fukagawa, C.A. Herzog, L. McCann, S. M. Moe, R. Shroff, M.A. Tonelli, N.D. Toussaint, et al., Diagnosis, evaluation, prevention, and treatment of chronic kidney disease-mineral and bone disorder: synopsis of the kidney disease: improving global outcomes 2017 clinical practice guideline update, *Ann. Intern. Med.* 168 (6) (2018) 422–430.
- [2] D.L. Andress, D.W. Coyne, K. Kalantar-Zadeh, M.E. Molitch, F. Zangeneh, S. M. Sprague, Management of secondary hyperparathyroidism in stages 3 and 4 chronic kidney disease, *Endocr. Pract.* 14 (1) (2008) 18–27.
- [3] T. Isakova, T.L. Nickolas, M. Denburg, S. Yarlagadda, D.E. Weiner, O.M. Gutiérrez, V. Bansal, S.E. Rosas, S. Nigwekar, J. Yee, et al., KDOQI US commentary on the 2017 KDIGO clinical practice guideline update for the diagnosis, evaluation, prevention, and treatment of chronic kidney disease-mineral and bone disorder (CKD-MBD), *Am. J. Kidney Dis. : Off. J. Nat. Kidney Found.* 70 (6) (2017) 737–751.
- [4] S.N. Salam, A. Khwaja, M.E. Wilkie, Pharmacological management of secondary hyperparathyroidism in patients with chronic kidney disease, *Drugs* 76 (8) (2016) 841–852.
- [5] A. Levin, G.L. Bakris, M. Molitch, M. Smulders, J. Tian, L.A. Williams, D.L. Andress, Prevalence of abnormal serum vitamin D, PTH, calcium, and phosphorus in patients with chronic kidney disease: results of the study to evaluate early kidney disease, *Kidney Int.* 71 (1) (2007) 31–38.
- [6] J. Cunningham, F. Locatelli, M. Rodriguez, Secondary hyperparathyroidism: pathogenesis, disease progression, and therapeutic options, *Clin. J. Am. Soc. Nephrol. : CJASN* 6 (4) (2011) 913–921.
- [7] L. Magagnoli, P. Ciceri, M. Cozzolino, Secondary hyperparathyroidism in chronic kidney disease: pathophysiology, Current treatments and investigational drugs, *Expert Opin. Invest. Drugs* 33 (8) (2024) 775–789.
- [8] R. Schneider, D.K. Bartsch, Role of surgery in the treatment of renal secondary hyperparathyroidism, *Br. J. Surg.* 102 (4) (2015) 289–290.
- [9] M. Bartz-Kurycki, S. Dream, Surgical management of secondary and tertiary hyperparathyroidism, *Surg. Clin.* 104 (4) (2024) 825–835.
- [10] U. Chilakamarthi, L. Giribabu, Photodynamic therapy: past, present and future, *Chem. Rec.* 17 (8) (2017) 775–802.
- [11] R.F. Lopez, N. Lange, R. Guy, M.V. Bentley, Photodynamic therapy of skin cancer: controlled drug delivery of 5-ALA and its esters, *Adv. Drug Deliv. Rev.* 56 (1) (2004) 77–94.
- [12] M. Overchuk, R.A. Weersink, B.C. Wilson, G. Zheng, Photodynamic and photothermal therapies: synergy opportunities for nanomedicine, *ACS Nano* 17 (9) (2023) 7979–8003.
- [13] S.A. Asher, G.E. Peters, S.F. Pehler, K. Zinn, J.R. Newman, Rosenthal EL: fluorescent detection of rat parathyroid glands via 5-aminolevulinic acid, *Laryngoscope* 118 (6) (2008) 1014–1018.

- [14] M. Przygoda, D. Bartusik-Aebisher, K. Dynarowicz, G. Ciešlar, A. Kawczyk-Krupka, D. Aebisher, Cellular mechanisms of singlet oxygen in photodynamic therapy, *Int. J. Mol. Sci.* 24 (23) (2023).
- [15] M. Ali-Seyed, R. Bhuvaneshwari, K.C. Soo, M. Olivo, Photolon™ –photosensitization induces apoptosis via ROS-mediated cross-talk between mitochondria and lysosomes, *Int. J. Oncol.* 39 (4) (2011) 821–831.
- [16] Y. Lu, W. Sun, J. Du, J. Fan, X. Peng, Immuno-photodynamic therapy (IPDT): organic photosensitizers and their application in cancer ablation, *JACS Au* 3 (3) (2023) 682–699.
- [17] B.J. Mossakowska, A. Fabisiewicz, B. Tudek, J.A. Siedlecki, Possible mechanisms of resistance development to photodynamic therapy (PDT) in vulvar cancer cells, *Int. J. Mol. Sci.* 23 (23) (2022).
- [18] T.P. Kacso, R. Zahu, A. Tirpe, E.V. Paslari, A. Nuțu, I. Berindan-Neagoe, Reactive oxygen species and long non-coding RNAs, an unexpected crossroad in cancer cells, *Int. J. Mol. Sci.* 23 (17) (2022).
- [19] J. Zuo, Z. Zhang, M. Li, Y. Yang, B. Zheng, P. Wang, C. Huang, S. Zhou, The crosstalk between reactive oxygen species and noncoding RNAs: from cancer code to drug role, *Mol. Cancer* 21 (1) (2022) 30.
- [20] W. Ye, J. Ma, F. Wang, T. Wu, M. He, J. Li, R. Pei, L. Zhang, Y. Wang, J. Zhou, LncRNA MALAT1 regulates miR-144-3p to facilitate epithelial-mesenchymal transition of lens epithelial cells via the ROS/NRF2/Notch1/Snai1 pathway, *Oxid. Med. Cell. Longev.* 2020 (2020) 8184314.
- [21] A.Y. Wang, T. Akizawa, S. Bavanandan, T. Hamano, A. Liew, K.C. Lu, D. Lumlertgul, K.H. Oh, M.H. Zhao, S. Ka-Shun Fung, et al., Kidney disease: improving global outcomes (KDIGO) chronic kidney disease-mineral and bone disorder (CKD-MBD) guideline update implementation: asia summit conference report, *Kidney Intern. Rep.* 4 (11) (2017) 1523–1537, 2019.
- [22] L. Zeng, Q. Zou, P. Huang, L. Xiong, Y. Cheng, Q. Chen, Y. Li, H. He, W. Yi, W. Wei, Inhibition of autophagy with Chloroquine enhanced apoptosis induced by 5-aminolevulinic acid-photodynamic therapy in secondary hyperparathyroidism primary cells and organoids, *Biomed. pharmacotherapy* 142 (2021) 111994.
- [23] Y. Wen, L. Zeng, Q. Chen, Y. Li, M. Fu, Z. Wang, H. Liu, X. Li, P. Huang, W. Wu, et al., RNA-Seq-based transcriptomics analysis during the photodynamic therapy of primary cells in secondary hyperparathyroidism, *Photochem. Photobiol. Sci. : Offic. J. European Photochem. Assoc. European Soc. Photobio.* 22 (4) (2023) 905–917.
- [24] T. Saito, M. Mizobuchi, M. Sakai, T. Kawata, T. Kitayama, T. Kato, T. Suzuki, H. Ogata, F. Koiva, H. Honda, Effects of evocalcet on parathyroid calcium-sensing receptor and vitamin D receptor expression in uremic rats, *Faseb. J.* 37 (8) (2023) e23094 official publication of the Federation of American Societies for Experimental Biology.
- [25] T. Miyakogawa, G. Kanai, R. Tatsumi, H. Takahashi, K. Sawada, T. Kakuta, M. Fukagawa, Feasibility of photodynamic therapy for secondary hyperparathyroidism in chronic renal failure rats, *Clin. Exp. Nephrol.* 21 (4) (2017) 563–572.
- [26] H. Zheng, X. Liang, Q. Han, Z. Shao, Y. Zhang, L. Shi, Y. Hong, W. Li, C. Mai, Q. Mo, et al., Hemin enhances the cardioprotective effects of mesenchymal stem cell-derived exosomes against infarction via amelioration of cardiomyocyte senescence, *J. Nanobiotechnol.* 19 (1) (2021) 332.
- [27] Z. Gao, Z. Zhang, D. Gu, Y. Li, K. Zhang, X. Dong, L. Liu, J. Zhang, J. Chen, D. Wu, et al., Hemin mitigates contrast-induced nephropathy by inhibiting ferroptosis via HO-1/Nrf2/GPX4 pathway, *Clin. Exp. Pharmacol. Physiol.* 49 (8) (2022) 858–870.
- [28] H.E. Choi, E.J. Jeon, D.Y. Kim, M.J. Choi, H. Yu, J.I. Kim, H.G. Cheon, Sodium salicylate induces browning of white adipocytes via M2 macrophage polarization by HO-1 upregulation, *Eur. J. Pharmacol.* 928 (2022) 175085.
- [29] Y. Bian, Y. Chen, X. Wang, G. Cui, C.O.L. Ung, J.H. Lu, W. Cong, B. Tang, S.M. Lee, Oxyphylla A ameliorates cognitive deficits and alleviates neuropathology via the Akt-GSK3 $\beta$  and Nrf2-Keap1-HO-1 pathways in vitro and in vivo murine models of Alzheimer's disease, *J. Adv. Res.* 34 (2021) 1–12.
- [30] J. Xu, K.C. Yang, N.E. Go, S. Colborne, C.J. Ho, E. Hosseini-Beheshti, A.H. Lystad, A. Simonsen, E.T. Guns, G.B. Morin, et al., Chloroquine treatment induces secretion of autophagy-related proteins and inclusion of Atg8-family proteins in distinct extracellular vesicle populations, *Autophagy* 18 (11) (2022) 2547–2560.
- [31] H.L. Wang, J.N. Li, W.J. Kan, G.Y. Xu, G.H. Luo, N. Song, W.B. Wu, B. Feng, J.F. Fu, Y.T. Tu, et al., Chloroquine enhances the efficacy of chemotherapy drugs against acute myeloid leukemia by inactivating the autophagy pathway, *Acta Pharmacol. Sin.* 44 (11) (2023) 2296–2306.
- [32] N. Guo, Z. Peng, MG132, a proteasome inhibitor, induces apoptosis in tumor cells, *Asia Pac. J. Clin. Oncol.* 9 (1) (2013) 6–11.
- [33] M. Aires-Fernandes, R. Botelho Costa, S. Rochetti do Amaral, C.U. Mussagy, V. C. Santos-Ebinuma, F.L. Primo, Development of biotechnological photosensitizers for photodynamic therapy: cancer research and treatment-from benchtop to clinical practice, *Molecules* 27 (20) (2022).
- [34] A.-G. Niculescu, A.M. Grumezescu, Photodynamic therapy—an up-to-date review, *Appl. Sci.* 11 (8) (2021) 3626.
- [35] H.J. Nyst, I.B. Tan, F.A. Stewart, A.J. Balm, Is photodynamic therapy a good alternative to surgery and radiotherapy in the treatment of head and neck cancer? Photodiagnosis Photodyn. Ther. 6 (1) (2009) 3–11.
- [36] A. Kawczyk-Krupka, A.M. Bugaj, W. Latos, K. Zaremba, K. Wawrzyniec, M. Kucharzewski, A. Sieroń, Photodynamic therapy in colorectal cancer treatment—The state of the art in preclinical research, *Photodiagnosis Photodyn. Ther.* 13 (2016) 158–174.
- [37] N. Hodgkinson, C.A. Kruger, H. Abrahamse, Targeted photodynamic therapy as potential treatment modality for the eradication of colon cancer and colon cancer stem cells, *Tumour biology : J. Intern. Soc. Oncodev. Biol. Med.* 39 (10) (2017) 1010428317734691.
- [38] J.A. Rodrigues, J.H. Correia, Photodynamic therapy for colorectal cancer: an update and a look to the future, *Int. J. Mol. Sci.* 24 (15) (2023) 12204.
- [39] D. Xu, W. Wang, D. Wang, J. Ding, Y. Zhou, W. Zhang, Long noncoding RNA MALAT-1: a versatile regulator in cancer progression, metastasis, immunity, and therapeutic resistance, *Non-coding RNA research* 9 (2) (2024) 388–406.
- [40] S. Meng, B. Wang, W. Li, LncRNA MALAT1 improves cerebral ischemia-reperfusion injury and cognitive dysfunction by regulating miR-142-3p/SIRT1 axis, *Int. J. Neurosci.* 133 (7) (2023) 740–753.
- [41] E.H.M. Hassanein, I.M. Ibrahim, E.K. Abd-Alhameed, Z.W. Sharawi, F.A. Jaber, H. S. Althagafy, Nrf2/HO-1 as a therapeutic target in renal fibrosis, *Life Sci.* 334 (2023) 122209.
- [42] Y. Fang, C. Xing, X. Wang, H. Cao, C. Zhang, X. Guo, Y. Zhuang, R. Hu, G. Hu, F. Yang, Activation of the ROS/HO-1/NQO1 signaling pathway contributes to the copper-induced oxidative stress and autophagy in duck renal tubular epithelial cells, *Sci. Total Environ.* 757 (2021) 143753.
- [43] T. Liu, C.Y. Li, H. Chen, J. Liu, L.L. Zhong, M.M. Tang, W.B. Wang, J.P. Huang, X. S. Jiang, TBHQ attenuates podocyte injury in diabetic nephropathy by inhibiting NADPH oxidase-derived ROS generation via the Nrf2/HO-1 signalling pathway, *Heliyon* 8 (9) (2022) e10515.
- [44] L.E. Otterbein, R. Foresti, R. Motterlini, Heme oxygenase-1 and carbon monoxide in the heart: the balancing act between danger signaling and pro-survival, *Circ. Res.* 118 (12) (2016) 1940–1959.
- [45] X. Dang, B. He, Q. Ning, Y. Liu, J. Guo, G. Niu, M. Chen, Alantolactone suppresses inflammation, apoptosis and oxidative stress in cigarette smoke-induced human bronchial epithelial cells through activation of Nrf2/HO-1 and inhibition of the NF- $\kappa$ B pathways, *Respir. Res.* 21 (1) (2020) 95.
- [46] D.D. Zhang, M. Hannink, Distinct cysteine residues in Keap1 are required for Keap1-dependent ubiquitination of Nrf2 and for stabilization of Nrf2 by chemopreventive agents and oxidative stress, *Mol. Cell Biol.* 23 (22) (2003) 8137–8151.
- [47] K. Taguchi, H. Motohashi, M. Yamamoto, Molecular mechanisms of the Keap1–Nrf2 pathway in stress response and cancer evolution, *Gene Cell. : Devo. Mole. Cell. Mechan.* 16 (2) (2011) 123–140.
- [48] R. Zeng, R. Zhang, X. Song, L. Ni, Z. Lai, C. Liu, W. Ye, The long non-coding RNA MALAT1 activates Nrf2 signaling to protect human umbilical vein endothelial cells from hydrogen peroxide, *Biochem. Biophys. Res. Commun.* 495 (4) (2018) 2532–2538.
- [49] I. Bellezza, I. Giambanco, A. Minelli, R. Donato, Nrf2-Keap1 signaling in oxidative and reductive stress, *Biochim. Biophys. Acta Mol. Cell Res.* 1865 (5) (2018) 721–733.
- [50] N. Amodio, M.A. Stamato, G. Juli, E. Morelli, M. Fulciniti, M. Manzoni, E. Taiana, L. Agnelli, M.E.G. Cantafio, E. Romeo, et al., Drugging the lncRNA MALAT1 via LNA gapter ASO inhibits gene expression of proteasome subunits and triggers anti-multiple myeloma activity, *Leukemia* 32 (9) (2018) 1948–1957.
- [51] R. Radhakrishnan, R.A. Kowluru, Long noncoding RNA MALAT1 and regulation of the antioxidant defense system in diabetic retinopathy, *Diabetes* 70 (1) (2021) 227–239.
- [52] J.W. Xin, Y.G. Jiang, Long noncoding RNA MALAT1 inhibits apoptosis induced by oxygen-glucose deprivation and reoxygenation in human brain microvascular endothelial cells, *Exp. Ther. Med.* 13 (4) (2017) 1225–1234.
- [53] S.W. Ryter, K. Mizumura, A.M. Choi, The impact of autophagy on cell death modalities, *Int. J. Cell. Biol.* 2014 (2014) 502676.
- [54] M. Su, Y. Mei, S. Sinha, Role of the crosstalk between autophagy and apoptosis in cancer, *JAMA Oncol.* 2013 (2013) 102735.